2003

Buried Ion-Exchanged Glass Wavelengths: Burial-Depth Dependence on Waveguide Width

P. Madasamy
University of Arizona

Brian R. West
Wilfrid Laurier University, bwest@wlu.ca

Michael M. Morrell
Unviersity of Arizona

David F. Geraghty
Unviersity of Arizona

Seppo Honkanen
University of Arizona

See next page for additional authors

Buried ion-exchanged glass waveguides: burial-depth dependence on waveguide width

P. Madasamy, B. R. West, M. M. Morrell, D. F. Geraghty, S. Honkanen, and N. Peyghambarian

Optical Sciences Center, University of Arizona, 1630 East University Boulevard, Tucson, Arizona 85721

Received January 27, 2003

A detailed theoretical and experimental study of the depth dependence of buried ion-exchanged waveguides on waveguide width is reported. Modeling, which includes the effect of nonhomogeneous time-dependent electric field distribution, agrees well with our experiments showing that burial depth increases linearly with waveguide width. These results may be used in the proper design of integrated optical circuits that need waveguides of different widths at different sections, such as arrayed waveguide gratings. © 2003 Optical Society of America

OCIS codes: 130.0130, 230.7390, 290.1990, 000.4430.

Buried silver-ion-exchanged glass waveguides are used extensively in integrated optical devices for optical communications because they feature very low loss, are well matched with single-mode fibers, and can have negligible birefringence.[1–3] These buried channel waveguides are fabricated by first performing a thermal silver-ion exchange through a mask patterned on the glass surface. At the surface silver ions are exchanged for sodium ions, and the refractive index is locally increased. The resulting surface channel waveguides are then buried by an electric-field-assisted, unmasked ion exchange. In this step the silver ions migrate deeper into the glass, and the waveguides are buried below the glass surface.

In many cases it is necessary to use waveguides of different widths in different sections of an integrated optical circuit. Good examples of such devices are arrayed waveguide gratings[4] and devices based on multimode interference.[5] If these devices are fabricated with buried ion-exchanged waveguides, significant losses are expected due to vertical waveguide misalignment at the junction between two waveguides with different widths. It has been suggested[6] that the burial depth would be different for a channel waveguide and a slab waveguide with no lateral confinement.

In this Letter we report on a detailed study of the dependence of the burial depth on the initial mask-opening width in the case of buried silver-ion-exchanged glass waveguides. We first present the results of our theoretical modeling, which takes into account the nonhomogeneous time-dependent electric field distribution in glass during the burial process. Then we describe a simple technique that we developed to accurately measure the burial depths of fabricated waveguides. The experimental results are in good agreement with our modeling, and we show that the burial depth increases with increasing waveguide width. This behavior is explained by the different mobilities of silver and sodium ions in the glass used in the experiments.

A binary ion exchange, such as Ag^+-Na^+ exchange, involves a system with two kinds of monovalent ions: indiffusing ions (A) and outdiffusing ions (B) in the glass substrate. There are two types of force that drive the exchange of ions. One is due to the concentration gradient of ions (diffusion) and the other is due to the drift of ions resulting from the electric field in the glass during the exchange. The electric field can be an externally applied field or an internal field built by the local charge imbalances caused by the difference in mobilities of the exchanging ions.

The development of concentration distribution in time can be given by[7]

$$\frac{\partial C_A}{\partial t} = \frac{D_A}{1 \quad \alpha C_A}\left[\nabla^2 C_A + \frac{\alpha(\nabla C_A)^2}{1 \quad \alpha C_A} \quad \frac{e\mathbf{E}_{\text{ext}}\nabla C_A}{kT}\right]. \tag{1}$$

The first two terms result from the concentration gradient of ions and the internal field due to the local distribution of ions with different mobilities, respectively. The third term results from the external applied electric field. Here $C_A = c_A/c_o$ is the normalized concentration of A ions, where c_A is the ionic concentration of A ions and c_o is the total ionic concentration. D_A and D_B are the self-diffusion coefficients of A ions and B ions, respectively, and $\alpha = 1 \quad D_A/D_B$ is a measure of the difference in ion mobilities. $D_A/(1 \quad \alpha C_A)$ is the interdiffusion coefficient, which for small values of M (the ratio between the self-diffusion coefficient of two ions, D_A/D_B) is strongly concentration dependent.

To solve Eq. (1), usually a time-independent current with homogeneous conductivity in the glass is assumed. However, it has been reported[8,9] that the inhomogeneity of the conductivity due to the exchanged ions perturbs the field and results in variations in the concentration profile. Since these variations can affect the burial depth of a waveguide mode and the effect of field perturbations will be slightly different for different mask-opening widths, the inhomogeneity in conductivity has to be taken into account in the modeling. We follow the approach of Ref. 8 to obtain the nonhomogeneous field distribution. The field has to be evaluated for each time step and inserted into Eq. (1), which is then solved by the Peaceman–Rachford alternating direction implicit method.

0146-9592/03/131132-03$15.00/0

In our calculations we use the diffusion parameters and refractive indices estimated for 3-in. BGG31 glass substrates (1 in. = 2.54 cm). These values were obtained from slab waveguide and prism-coupling experiments.[10] To study the burial-depth dependence on the mask-opening width, the same process parameters were used to simulate eight buried waveguides with different mask-opening widths during the first step, ranging from 2 to 9 μm. The estimated self-diffusion coefficient of silver ions is 1×10^{-15} m^2/s at $T = 553$ K and 3.5×10^{-16} m^2/s at $T = 523$ K. The value of M for the glass is 0.2. The first step, thermal ion exchange, is done for 4500 s at $T = 553$ K. The second step, field-assisted burial, is done for 2400 s at $T = 523$ K with an applied voltage of $U = 3.2$ V across the 20-μm-thick substrate. The small values used for voltage and thickness correspond to the values of 320 V and 2 mm used in the experiment. Note that a small value for the thickness of the glass is used to reduce the number of points in the calculation; the modeling results would not be different if we used a larger substrate thickness and correspondingly larger voltages.

We define the burial depth of the waveguide in terms of the mode profile since that is more relevant in practical applications. The mode profile of the waveguide was solved by the scalar finite-difference method, with a substrate index of 1.4525 at 1.55 μm and a maximum index change of 0.03. Figure 1 gives the concentration and intensity profiles of waveguides with 3- and 9-μm mask-opening widths. The electric field lines shown with the concentration profiles clearly demonstrate that the field lines deviate from the homogeneous case.

For comparison with the experiments done using a fiber, we take a convolution of the waveguide mode profile and a Gaussian function approximating the fiber mode. The distance from the surface of the glass to the peak of the convolution is defined as the burial depth of the waveguide. The results of the burial-depth modeling as a function of mask-opening width are given in Fig. 2. The error bars are a result of the finite grid spacing. For $M = 0.2$ the burial depth increases linearly with the mask-opening width. This behavior can be explained from the strong concentration dependence of the interdiffusion coefficient for small values of M, which affects the drift velocity of the peak concentration of waveguides during the burial step. It should be noted that even though the diffusion depth in terms of concentration changes with the mask-opening width after the first step, as has been similarly observed in other studies,[11–13] the waveguide depth in terms of the mode profile does not change with the mask-opening width. This difference in diffusion depths does not influence the burial depths, as can be seen from the case for $M = 1$, where there is no concentration dependence on the interdiffusion coefficient, and there is no difference in burial depth for different mask openings. When waveguides formed from different mask-opening widths are buried, the concentration values of the narrower waveguides become smaller faster since the gradient in the transverse direction is larger for narrower waveguides. The interdiffusion coefficient is larger for higher concentrations, and hence the wider waveguides become buried deeper than the narrower waveguides. The results for $M = 0.5$ and $M = 1$ are also plotted in Fig. 2. The concentration dependence of the interdiffusion coefficient is stronger for smaller M and disappears for $M = 1$. Hence the slope of the variation in burial depth is larger for $M = 0.2$ than for $M = 0.5$, and there is no variation in burial depth for $M = 1$.

To experimentally investigate burial-depth dependence on waveguide width, we fabricated buried waveguides in BGG31 glass and used parameters similar to those used in modeling. Mask widths ranging from 2 to 9 μm were patterned onto the sample. The first step, thermal ion exchange, was performed in a 50:50 $AgNO_3/NaNO_3$ melt at $T = 553$ K for 4500 s. The second step, unmasked field-assisted burial, was done at $T = 523$ K for 2400 s, with an applied

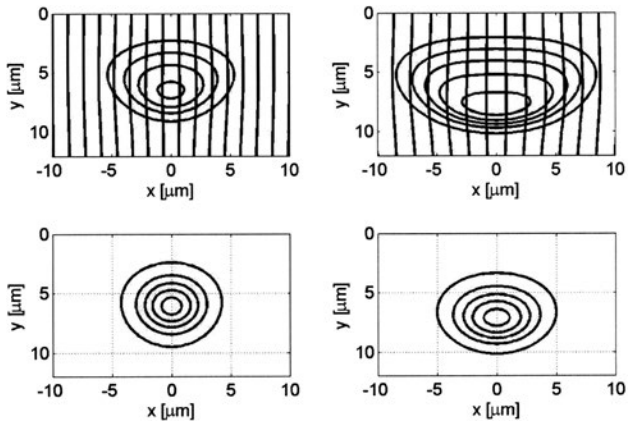

Fig. 1. Concentration profile with the electric field lines at the end of the burial process for the 3- and 9-μm waveguides are given in the top row with the 3-μm waveguide on the left and the 9-μm waveguide on the right. The contours for the concentration profile represent the relative silver-ion concentration and go as $0.1, 0.2, \ldots, 0.4$ for the 3-μm waveguide and $0.1, 0.2, \ldots, 0.5$ for the 9-μm waveguide. The corresponding intensity profiles solved by the finite-difference method are given below the concentration profiles. The contour lines for the intensity profile go as $0.1, 0.3, \ldots, 0.9$ of the normalized intensity.

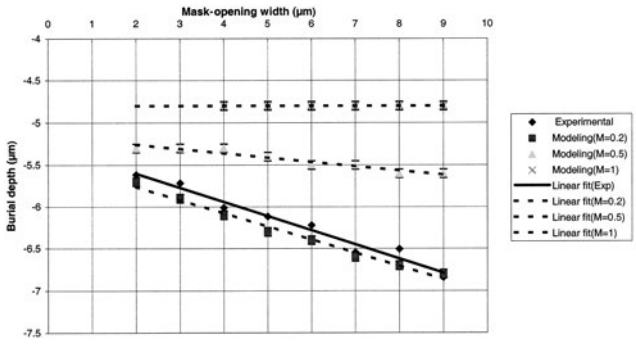

Fig. 2. Burial-depth variation as a function of mask-opening width. The solid line corresponds to the linear fit for the experimental data, and the dashed lines correspond to the linear fit for the modeled data.

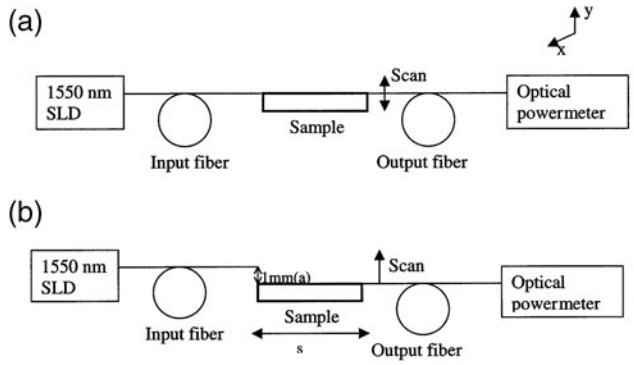

Fig. 3. Experimental setup for measuring burial depth based on the Newport AutoAlign System.

voltage of 320 V across a 2-mm substrate thickness. Taking advantage of the high accuracy of the Newport AutoAlign system, we developed a simple procedure for measuring the burial depth.[14] The data were taken with a resolution of 0.1 μm. The measurement consists of two steps: one is to find the center of the mode, and the other is to find the surface of the glass relative to the center of the mode. The setup used to find the center of the mode is given in Fig. 3(a). The input fiber from a 1550-nm superluminescent diode source and the output fiber to the optical power meter are butt coupled to the waveguide, and the throughput is maximized. Then the output fiber is scanned in the vertical y direction, and the center of the profile gives the center of the mode (y_0). To find the surface of the glass the input fiber is moved about 1 mm from it, as shown in Fig. 3(b). This forms a Lloyd's mirror interferometerlike setup with interference fringes formed because of the direct light from the input fiber and the reflected light from the glass surface. The intensity in the y direction in the observation plane is $I = 4I_0 \sin^2(\pi a y/s\lambda)$ for $y > 0$, where $y = 0$ corresponds to the surface. The interference fringe has a minimum at the surface of the glass, and there are no fringes below the surface. In the setup in Fig. 3(b) scanning the output fiber in the y direction from the center of the mode gives the fringes, and the first minimum gives the surface point. The difference between the surface point and the center of the mode gives the burial depth for the waveguide. The experimental results are plotted in Fig. 2. The results agree well with the modeling results for $M = 0.2$.

In conclusion, we studied the variations in burial depths of modes in ion-exchanged glass waveguides for different mask-opening widths. We did an accurate modeling, including the effect of nonhomogeneous electric field distribution in glass, and found the burial depths to vary linearly as a function of mask-opening width. We developed a simple setup to measure the burial depth and measured them in a sample fabricated with parameters similar to those used in the modeling. The experimental results were found to agree well with the modeling. The difference in burial depths arises largely from the concentration dependence of the interdiffusion coefficient when M (the ratio of self-diffusion coefficients D_A and D_B) is less than 1. This behavior of ion-exchanged glass waveguides must be taken into account when designing integrated optical circuits. The loss at the intersection of a narrow and a wide waveguide can be eliminated by adding a proper taper at the intersection. Also, as seen from the modeling results, the difference in burial depths becomes negligible for values of M close to 1. Therefore the use of glass with M close to 1 will eliminate the difference in burial depths caused by different mask-opening widths.

We acknowledge support from the Center for Optoelectronic Devices, Interconnects, and Packaging and the Technology and Research Initiative Fund. P. Madasamy's e-mail address is pmadasamy@optics.arizona.edu.

References

1. S. Honkanen, Proc. SPIE **53,** 159 (1994).
2. Y. Jaouen, L. du-Mouza, D. Barbier, J. M. Delavaux, and P. Bruno, IEEE Photon. Technol. Lett. **11,** 1105 (1999).
3. D. F. Geraghty, D. Provenzano, M. M. Morrell, S. Honkanen, A. Yariv, and N. Peyghambarian, Electron. Lett. **37,** 829 (2001).
4. K. Okamoto, M. Moriwaki, and S. Suzuki, Electron. Lett. **31,** 184 (1995).
5. L. H. Spiekman, Y. S. Oei, E. G. Metaal, F. H. Groen, I. Moerman, and M. K. Smit, IEEE Photon. Technol. Lett. **6,** 1008 (1994).
6. B. Buchold and E. Voges, Electron. Lett. **32,** 2249 (1996).
7. J. Albert and J. W. Y. Lit, Appl. Opt. **29,** 2798 (1990).
8. D. Cheng, J. Saarinen, H. Saarikoski, and A. Tervonen, Opt. Commun. **137,** 233 (1997).
9. Jerome Hazart and V. Minier, IEEE J. Quantum Electron. **37,** 606 (2001).
10. R. G. Walker, C. D. W. Wilkinson, and J. A. H. Wilkinson, Appl. Opt. **22,** 1923 (1983).
11. R. V. Ramaswamy and R. Srivastava, J. Lightwave Technol. **6,** 984 (1988).
12. M. N. Weiss and R. Srivastava, Appl. Opt. **34,** 455 (1995).
13. L. Palchetti, E. Giorgetti, D. Grando, and S. Sottini, IEEE J. Quantum Electron. **34,** 179 (1998).
14. P. Madasamy, M. M. Morrell, D. F. Geraghty, S. Honkanen, and N. Peyghambarian, in *Technical Digest: Symposium on Optical Fiber Measurements, 2002,* P. A. Williams and G. W. Day, eds. (National Institute for Standards and Technology, Boulder, Colo., 2002), pp. 25–28.